RSC Advances

PAPER

View Article Online
View Journal | View Issue

Cite this: *RSC Adv.*, 2017, **7**, 8852

Large-scale synthesis of uniformly loaded cobalt nanoparticles on alumina for efficient clean fuel production†

Ji Chan Park,*[ab] Jae In Kwon,[a] Shin Wook Kang,[a] Dong Hyun Chun,[ab] Ho-Tae Lee,[a] Heon Jung[a] and Jung-Il Yang*[a]

Received 14th December 2016
Accepted 22nd January 2017

DOI: 10.1039/c6ra28177j

rsc.li/rsc-advances

Large-scale synthesis of cobalt nanoparticles supported on alumina (Co/Al_2O_3), which has well dispersed metallic cobalt around 15 nm, was conducted *via* a simple melt infiltration process of a cobalt hydrate salt and subsequent thermal reduction. The catalytic performance of Co/Al_2O_3 was studied for Fischer–Tropsch synthesis in order to optimize the liquid fuel productivity for target hydrocarbon products controlled by reaction pressures and temperatures. The catalyst showed promising CO conversions up to 76% with high hydrocarbon productivity (~1.0 $g_{HC}\ g_{cat}^{-1}\ h^{-1}$) and good stability.

1. Introduction

Fischer–Tropsch synthesis (FTS) is a catalytic polymerization process for converting synthesis gas (a mixture of CO and H_2) into long-chain hydrocarbons to produce clean liquid fuels from fossil resources, such as natural gas, biomass or coal.[1–3] Especially, in the process of synthesis gas derived from natural gas, cobalt supported catalysts have been used because of their high FTS activity and selectivity for linear paraffins.[4] In recent years, selectivity control for the hydrocarbon products has been a big challenge in FTS.[5,6] For instance, for the selective production of gasoline-range hydrocarbon products (C_5–C_{12}), hybrid cobalt catalysts including zeolite compounds such as ZSM-5 as a cracking catalyst were exploited.[7,8] Until now, numerous studies on the preparation of cobalt-based FTS catalysts have been reported using various synthetic methods, such as sol–gel, impregnation, co-precipitation, deposition–precipitation, chemical vapour deposition and colloidal methods.[9] Typically, the preparation variables of metal/promoter loading, preparation method, pre-treatment, and so on, significantly affect the catalyst performance in FTS.[10–14]

Study on nano-catalysis has rapidly grown with the addition of new nanomaterials for various catalytic reactions.[15–19] Along this line, the development of nanostructured catalysts was conducted, not only for fundamental study using computational simulations or theoretical backgrounds, but also for industrial application.[20–22] Surface science studies, in particular, have contributed to fundamental understanding of nanostructured catalyst and catalysis.[23] However, in many cases, large-scale synthesis of nanocatalysts were still restricted by complex synthetic processes that were expensive and took much time, as well as by environmental problems caused by the use of harmful solvents. In particular, large-scale nanoparticle preparation by solution phase was very difficult.[24,25] In addition, the nanoparticles prepared using surfactants as stabilizer, have organic layers on their surface, sometimes retarding the activity of the catalyst.[26]

For these reasons, many commercial catalysts, so far, have been produced by a simple process involving mixing, shaking and baking process. It is needed to develop more economical and reproducible mass production methods for nanocatalyst having high activity and promising catalytic performance.

Recently, de Jong *et al.* reported the melt infiltration process as an emerging technique with no additional solvent use.[27] It could be utilized as a fast, convenient route to prepare various supported metal catalysts that contain small and well dispersed active nanoparticles inside robust supports. Herein, we demonstrate a simple and eco-friendly preparation method for mass production of Co/Al_2O_3 nanocatalyst, *via* a melt infiltration process without use of any organic solvent and an optimum thermal reduction condition. A commercially available alumina with high porosity and surface area was exploited as the support for large-scale production of the catalyst. The catalytic performance of the catalyst was optimized by conducting FTS reactions with control of the reaction conditions (10 and 20 bar, 230–260 °C). Without additional use of a cracking catalyst, the degree of carbon chain growth was controlled by the Co/Al_2O_3 nanocatalyst under varied reaction conditions. Under the optimum condition, the Co/Al_2O_3 nanocatalyst shows high FTS activity (~1.4×10^{-4} $mol_{CO}\ g_{Co}^{-1}\ s^{-1}$), with good stability.

[a]*Clean Fuel Laboratory, Korea Institute of Energy Research, 152 Gajeong-Ro, Daejeon, 34129, Republic of Korea. E-mail: jcpark@kier.re.kr; Tel: +82-42-860-3605*

[b]*Advanced Energy and Technology, University of Science and Technology, 217 Gajeong-Ro, Daejeon, 34113, Korea*

† Electronic supplementary information (ESI) available. See DOI: 10.1039/c6ra28177j

2. Experimental

2.1 Chemicals

Cobalt(II) nitrate hexahydrate ($Co(NO_3)_2 \cdot 6H_2O$, ACS reagent, ≥98%) was purchased from Sigma-Aldrich. A gamma-alumina powder was obtained from Strem Chemical, Inc. The chemicals were used as received without further purification.

2.2 Large-scale synthesis of Co/Al_2O_3 nanocatalyst

For the preparation of the Co/Al_2O_3 nanocatalyst with a theoretical Co load of 15 wt% in the reduced catalyst, 26.1 g of $Co(NO_3)_2 \cdot 6H_2O$ and 30.0 g of Al_2O_3 was physically mixed in a mortar for several minutes under ambient conditions, until the colour of the powder was homogeneously pink. The mixed powder was then aged in a polypropylene bottle at 60 °C in a tumbling oven. After aging for 24 h, the sample was cooled under an ambient atmosphere and transferred to an alumina crucible in a furnace. Finally, the cobalt-incorporated alumina powder was slowly heated at a ramping rate of 3.5 °C min^{-1} up to 450 °C under a hydrogen flow of 1.0 L min^{-1}. The sample was held at the same temperature for 4 h under hydrogen gas. After the thermal reduction, the Co/Al_2O_3 nanocatalyst was cooled to room-temperature and immediately submerged in ethanol (0.2 L) under a flow of nitrogen (1.0 L min^{-1}) in order to minimize surface oxidation of the cobalt particles. The black powder immersed in ethanol was simply separated by a magnet and dried in a vacuum oven at room temperature. The final Co/Al_2O_3 powder was pressed into pellets; then the resulting catalyst disk was crushed and sieved to yield 300–600 μm particles for a test in a fixed-bed reactor.

2.3 Fischer–Tropsch synthesis

Fischer–Tropsch synthesis reactions were performed in a down-flow fixed-bed stainless steel reactor tube with an inner diameter of 5 mm. Typically, the catalyst (0.5 g) was diluted with glass beads (425–600 μm, 2.5 g) to prevent hot-spot generation, and then loaded in the catalyst bed. The reaction was carried out at 230–260 °C under 10 and 20 bar for 48 h using a reactant gas ($H_2/CO = 2.0$, GHSV = 6.8 NL g_{cat}^{-1} h^{-1}). The composition of the outlet gases was analysed using a gas chromatograph (DS Science, iGC7200) equipped with a thermal conductivity detector (TCD) and a flame ionization detector (FID). The flow rates of the outlet gases were measured using a wet-gas flow meter (Shinagawa Co.). After FTS reaction for 48 h, the solid hydrocarbon products were collected in a hot trap (240 °C), and the liquid hydrocarbon products and water were collected in a cold trap (0 °C). The isolated wax and liquid products were analysed using an offline gas chromatograph (Agilent, 6890N) and the simulated distillation method (ASTM D2887).

2.4 Characterization

The catalysts were characterized using high-resolution transmission electron microscopy (HR-TEM, Tecnai TF30 ST), a titan double Cs corrected TEM (Titan cubed G2 60-300), and high resolution powder-XRD (Rigaku SmartLab). For TEM analysis, samples were prepared by putting a few drops of the corresponding colloidal solutions on lacey carbon-coated copper grids (Ted Pellar, Inc). Hydrogen chemisorption measurement was carried out using a Micromeritics ASAP 2020 C. Before measurement, the sample was heated in flowing hydrogen gas to 400 °C and was held at the same temperature for 10 h. The H_2 adsorption isotherm was measured at 35 °C. Nitrogen sorption isotherms were measured at −196 °C with a Tristar II 3020 surface area analyser. Before measurements, the samples were degassed in a vacuum at 300 °C for 4 h.

3. Results and discussion

3.1 Synthesis of Co/Al_2O_3 nanocatalyst

Scheme 1 demonstrates the simple procedure for synthesis of Co/Al_2O_3 nanocatalyst with photos of the corresponding materials. A gamma-phase alumina was chosen as support, because it can strongly interact with active nanoparticles, maintaining small cobalt crystallites.[28] Based on the pore volume of the alumina support used, cobalt nanoparticles were loaded to obtain uniform cobalt dispersion with the optimum Co content. Using a 0.87 $g_{cobalt\ salt}/g_{alumina}$ ratio, the active Co nanoparticles were successfully embedded in the porous alumina support. The Co-loading content after the final thermal treatment was calculated to be nominally 15 wt% on the basis of Co converted from the cobalt nitrate salt. First, the hydrated cobalt salt was melt-infiltrated into the alumina powder by grinding at room temperature with subsequent aging at 60 °C for 24 h in a tumbling oven. Next, the infiltrated cobalt salt inside the alumina pore was decomposed into tiny Co nanoparticles by thermal reduction at 450 °C under a flow of hydrogen. The high-angle annular dark-field scanning transmission electron microscopy (HAADF-STEM) image showed bright dots, indicating the Co nanoparticles in the porous alumina support (Fig. 1a). The elemental mapping of cobalt (red) and aluminium (green) demonstrated a uniform particle dispersion without any extremely agglomerated particles (Fig. 1b and e). TEM analysis also revealed the status of Co nanoparticles as black dots (Fig. 1c). The high-resolution TEM (HRTEM) image and corresponding Fourier-transform pattern represented single crystal of metallic cobalt with a distance of 0.205 nm between neighbouring fringes, which correspond to the (111) planes of face-centered-cubic cobalt (Fig. 1d). The average particle size was measured to be 15.2 ± 2.7 nm in the TEM images (Fig. 1c, S1,

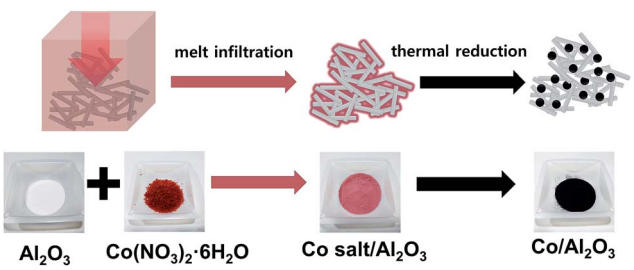

Scheme 1 A facile synthesis of Co/Al_2O_3 nanocatalyst by melt infiltration and thermal treatment.

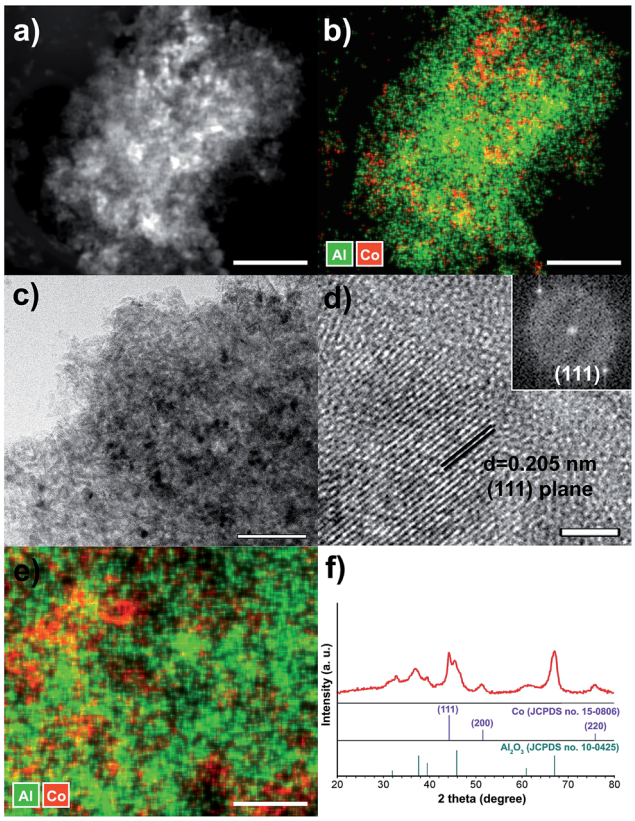

Fig. 1 (a) HADDF-TEM image, (b) low-resolution scanning-TEM image with elemental mapping of cobalt and aluminium, (c) TEM image, (d) HR-TEM image with the corresponding Fourier-transform pattern (inset of d), (e) magnified scanning-TEM image, and (f) XRD spectrum of Co/Al_2O_3 nanocatalyst. The bars represent 200 nm (a, b), 100 nm (c), 2 nm (d), and 10 nm (e).

ESI†). The X-ray diffraction (XRD) spectrum of Co/Al_2O_3 nanocatalyst matched to the metallic Co (JCPDS no. 15-0806; space group, $Fm\bar{3}m$) and gamma-phase Al_2O_3 (JCPDS no. 10-0425; space group, $Fd\bar{3}m$) (Fig. 1f). Major peaks of alumina were observed at $2\theta = 37.6°$, 45.9°, and 67.0°. The peak at $2\theta = 44.2°$, which was assigned to the reflections of the (111) plane in the fcc-Co, reflects tiny Co single-crystal domain sizes. The average size of the Co crystals was estimated to be 14.2 nm, from the broadness of the (111) peak using the Debye–Scherrer equation, which well-matched that observed in the TEM images. The average cobalt size of Co/Al_2O_3 nanocatalyst was also measured to be 17.1 nm, based on calculation of the Co dispersion (5.62%) obtained by H_2 chemisorption.

N_2 sorption experiments for pristine Al_2O_3 and the Co/Al_2O_3 nanocatalyst exhibited type IV adsorption–desorption hysteresis. The Brunauer–Emmett–Teller (BET) surface areas of the alumina and the Co/Al_2O_3 nanocatalyst were calculated to be 205 $m^2\ g^{-1}$ and 196 $m^2\ g^{-1}$, respectively (Fig. 2a). The total pore volume of the Co/Al_2O_3 nanocatalyst was found to be 0.31 $cm^3\ g^{-1}$, which is about 70% of the initial alumina (0.44 $cm^3\ g^{-1}$). The significant decrease in the pore volume of the Co/Al_2O_3 nanocatalyst was attributed to the cobalt occupancy. It demonstrates that the cobalt particles are mainly located inside

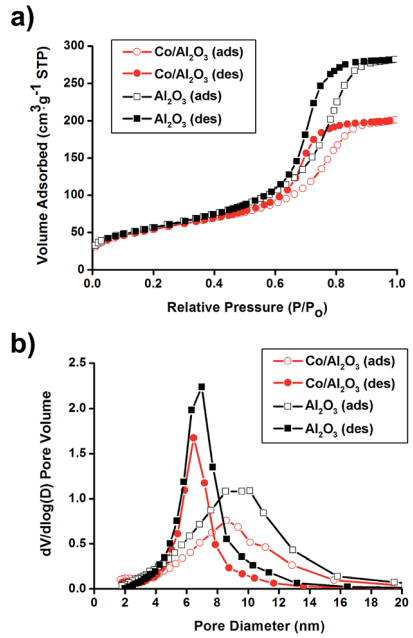

Fig. 2 (a) N_2 adsorption/desorption isotherms and (b) pore size distribution diagrams of pristine Al_2O_3 and Co/Al_2O_3 nanocatalyst.

the alumina pores, not on the outside. Applying the Barrett–Joyner–Halenda (BJH) method, the small pore sizes were obtained by the adsorption/desorption branches (Fig. 2b). Because of the occupancy of the alumina pores by the cobalt particles, the pore size in the Co/Al_2O_3 was also slightly decreased, compared to those of pristine Al_2O_3 (6.5 nm at the desorption branch and 8.6 nm at the adsorption branch).

3.2 Fischer–Tropsch synthesis reaction test

The catalytic activity of the synthesized Co/Al_2O_3 nanocatalyst was tested for the FTS reaction in a fixed bed reactor (Fig. 3). The reactions were carried out at 10 and 20 bar, 230–260 °C, with an H_2/CO ratio of '2'. In the reactions, CO conversion and hydrocarbon selectivity data were obtained for 48 h over time-on-stream (TOS) by analysing the gas chromatography data of the outlet gasses containing the unreacted CO, H_2, CH_4, C_2–C_4

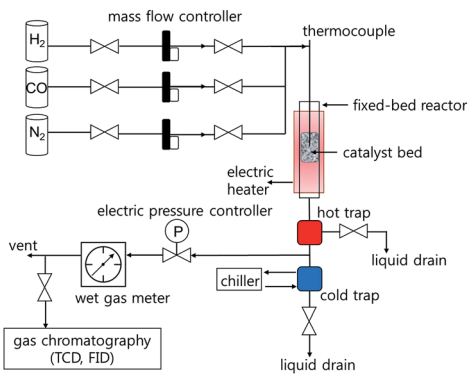

Fig. 3 Schematic diagram of Fischer–Tropsch synthesis reaction instruments.

hydrocarbons and CO_2. Because the active Co phase had been already generated during the catalyst preparation step before the FTS reaction, the Co/Al_2O_3 nanocatalyst could be directly employed in FTS without an additional *in situ* reduction/activation process. Under the same temperature conditions, higher CO conversions were measured at 20 bar than 10 bar (Fig. 4). This is, because higher reaction pressure can provide more beneficial conditions in FTS, as follows:

$$nCO + (2n + 1)H_2 \rightarrow C_nH_{2n+2} + nH_2O \text{ (paraffins)}$$

$$nCO + 2nH_2 \rightarrow C_nH_{2n} + nH_2O \text{ (olefins)}$$

Furthermore, the Co/Al_2O_3 nanocatalyst exhibited enhanced CO conversion with increased reaction temperature (230 to 260 °C) under the same reaction pressure condition. At 20 bar, the total CO conversion rates were observed to be 36.4% at 230 °C, 55.8% at 240 °C, 69.2% at 250 °C, and 76.0% at 260 °C, at TOS = 48 h. The highest CO conversion was obtained at 20 bar and 260 °C.

In the selectivity data, increase of the reaction pressure tends to increase C_{5+} selectivity and decrease CH_4 selectivity. This trend leads to the high yield of C_{5+} hydrocarbons (Fig. 5). Under 20 bar, the FTS reaction at 260 °C showed higher CO_2 (4.3%), CH_4 (24.0%), and C_2–C_4 (12.4%) selectivity and lower C_{5+} selectivity (59.3%) than at lower temperatures. The reaction at 230 °C showed low CO_2 (0.2%), CH_4 (13.5%) and C_2–C_4 (9.2%) selectivity, and high selectivity for C_{5+} (77.1%). Higher CO_2 concentrations in elevated reaction temperatures were mainly attributed to the increased water–gas shift (WGS) reaction as follows:

$$CO + H_2O \leftrightarrow CO_2 + H_2$$

The catalyst activity has been also noted in terms of the Cobalt-Time-Yield (CTY), *i.e.*, the number of CO moles converted to hydrocarbons per gram of cobalt per second over TOS. It can simply reflect the CO conversion and hydrocarbon

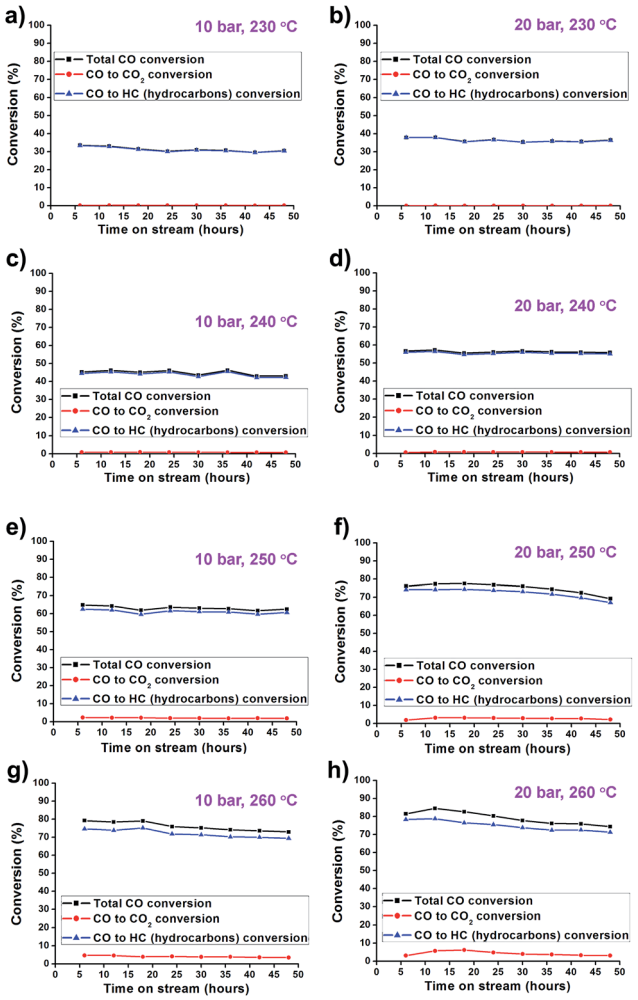

Fig. 4 (a–h) CO conversion graphs of Co/Al_2O_3 nanocatalyst at 10–20 bar and 230–260 °C. The total CO conversion is the sum of the CO conversion to hydrocarbons (CO to HC) and the CO conversion to CO_2 (CO to CO_2). The reaction tests were conducted at GHSV = 6.8 NL g_{cat}^{-1} h^{-1} and a H_2 : CO ratio of '2'.

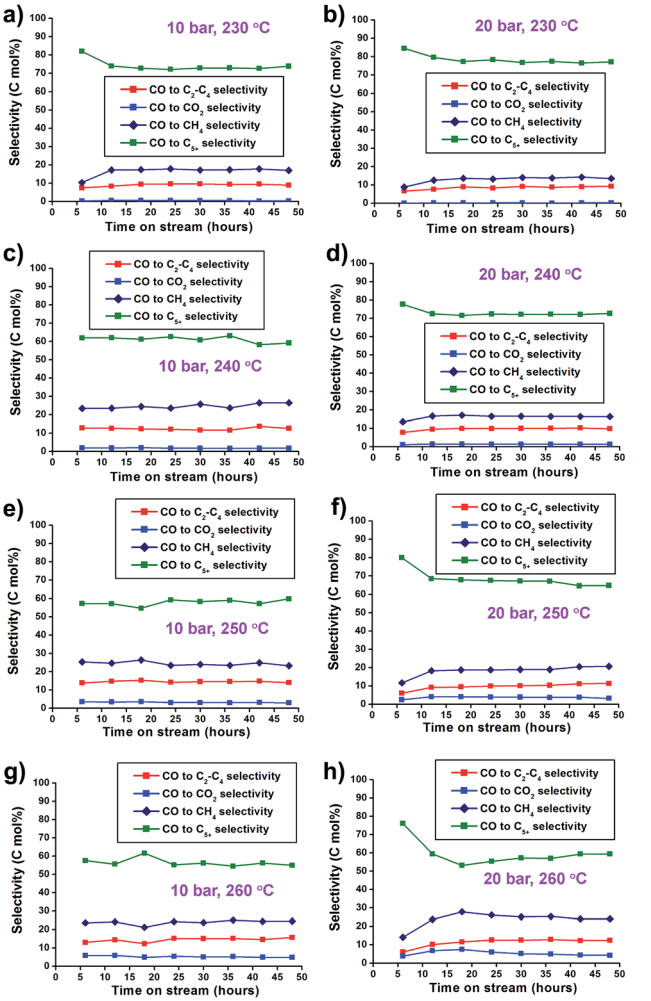

Fig. 5 (a–h) CO_2 and hydrocarbon selectivity graphs of Co/Al_2O_3 nanocatalyst at 10–20 bar and 230–260 °C. The reaction tests were conducted at GHSV = 6.8 NL g_{cat}^{-1} h^{-1} and a H_2 : CO ratio of '2'.

selectivity of catalysts for each FTS reaction condition. The Co/Al_2O_3 nanocatalyst showed good catalytic performance with high CTY values (Fig. 6). As expected, the catalyst used at the higher reaction temperature of 260 °C showed much higher CTY values than those of 230–250 °C. In particular, the CTY value at 20 bar and 260 °C was calculated to be 1.41×10^{-4} mol_{CO} g_{Co}^{-1} s^{-1} at TOS = 48 h, comparable with previously reported values of Co/Al_2O_3, Co/C, and Co/SiO_2 catalysts (Fig. 6b, Table S1†). Increase of the reaction pressure at the same reaction temperatures led to increased CTY values. Controlling temperature was more effective for increasing FTS activity than controlling the reaction pressure, and resulted in high CTY values.

The Co/Al_2O_3 nanocatalyst also showed very high productivity for hydrocarbon products. The specific hydrocarbon productivities were obtained from gas chromatography analysis of gaseous products and simulated distillation analysis of isolated solid and liquid products after FTS reactions (Fig. 7). At 20 bar and 260 °C, the maximum value of the total hydrocarbon (HC) productivity from C_1 to C_{44} was found to be 1.0 g_{HC} g_{cat}^{-1} h^{-1}. As expected, higher productivity at 20 bar for liquid hydrocarbon (C_{5+}) was measured than at 10 bar. In the case of gasoline-range products (C_5–C_{12}), the maximum productivity (0.381 g_{HC} g_{cat}^{-1} h^{-1}) was observed under 20 bar at 260 °C (Fig. 7b). On the other hand, the maximum values for diesel-range products (C_{13}–C_{18}) and wax-range products (C_{19+}) were observed under 20 bar at 250 and 240 °C, respectively.

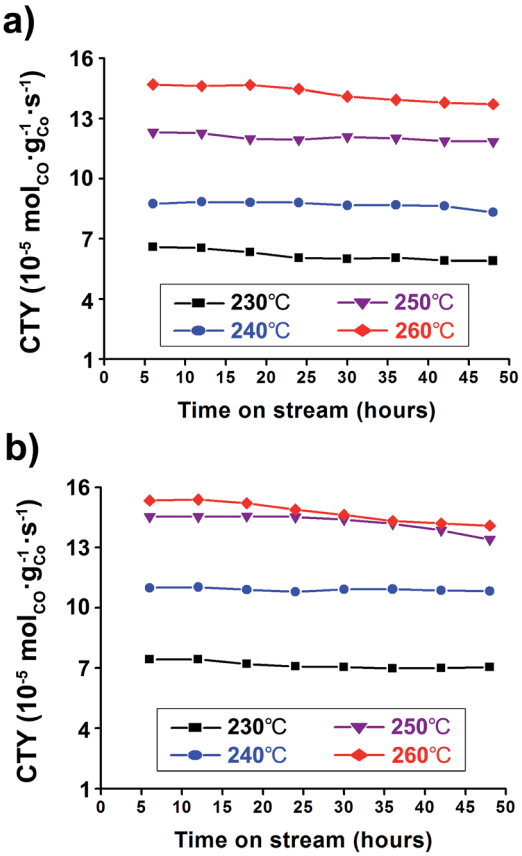

Fig. 6 Cobalt-Time-Yield (CTY) graphs conducted under 230–260 °C at (a) 10 bar and (b) 20 bar. The reaction tests were conducted at GHSV = 6.8 NL g_{cat}^{-1} h^{-1} and a H_2 : CO ratio of '2'.

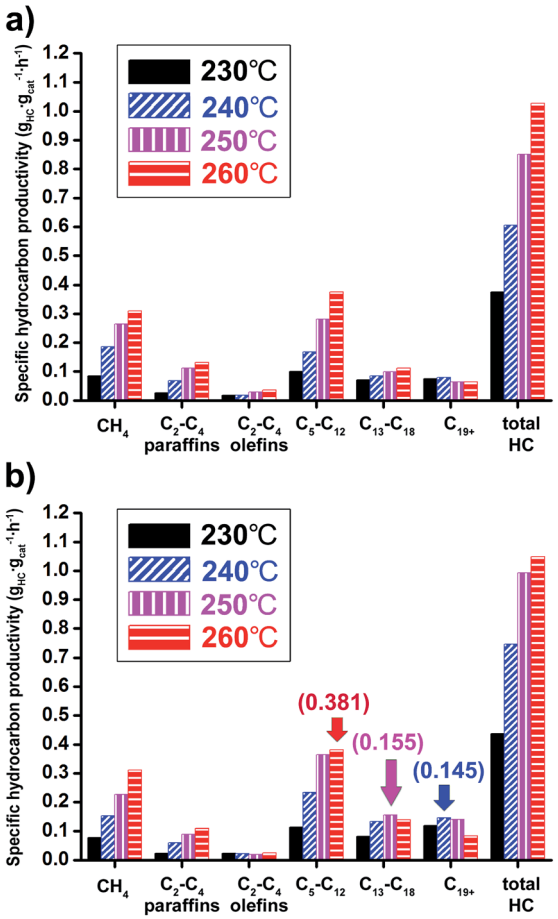

Fig. 7 Hydrocarbon productivity data of Co/Al_2O_3 nanocatalyst conducted under 230–260 °C at (a) 10 bar and (b) 20 bar. The reaction tests were conducted at GHSV = 6.8 NL g_{cat}^{-1} h^{-1} and a H_2 : CO ratio of '2'.

At 20 bar, the wax-range portion (C_{19+}) in total weight portions was significantly decreased with increase of reaction temperatures, indicating 27.1% at 230 °C and 8.0% at 260 °C (Table S2†). On the other hand, the gasoline-range portion (C_5–C_{12}) was increased (25.8% at 230 °C to 36.3% at 260 °C).

The chain growth probability (α) of the hydrocarbons can be calculated using the Anderson–Schulz–Flory (ASF) chain growth mechanism in the following equation:[29]

$$\log(W_n/n) = \log(\ln^2 \alpha) + n \log \alpha$$

where W_n is the weight fraction of hydrocarbons with carbon number n. The α values were obtained from the slope of the graph from C_5 to C_{44}. The high α value (0.885) at 230 °C and 20 bar indicate that the high pressure and low reaction temperature can provide more advantageous conditions for carbon chain growth on the catalyst (Table S3†). This value is apt to produce wax-range hydrocarbons (C_{19+}), but for the optimum production of diesel or gasoline range hydrocarbons, the α value should be lower. The obtained values of 0.848 at 250 °C

and 0.785 at 260 °C belong to optimal ranges of diesel (C_{13}–C_{18}) and gasoline (C_5–C_{12}) range hydrocarbon products, respectively.[30]

4. Conclusions

The Co nanoparticles (~15 nm) supported on alumina were simply prepared with tens of gram scale in a batch, *via* melt infiltration and subsequent thermal reduction. This route was reproducible, economically feasible, and eco-friendly. The Co/Al_2O_3 nanocatalyst, with supreme thermal stability and high Co dispersion, showed good CO conversion (~76%), very high CTY value (~1.4×10^{-4} mol_{CO} g_{Co}^{-1} s^{-1}) and remarkable hydrocarbon productivity (~1.0 g_{HC} g_{cat}^{-1} h^{-1}) under controlled FTS conditions. It is anticipated that the optimum reaction conditions for this catalyst could be effectively applied to commercial FTS for producing target liquid fuel products such as gasoline- and diesel-range hydrocarbons.

Acknowledgements

This research was supported by the Research and Development Program of the Korea Institute of Energy Research (KIER) (B6-2439) and funded by the Ministry of Trade, Industry and Energy (MOTIE) of the Republic of Korea (project no. 10050509).

Notes and references

1 M. E. Dry, *Catal. Today*, 2002, **71**, 227.
2 E. van Steen and M. Claeys, *Chem. Eng. Technol.*, 2008, **31**, 655.
3 A. de Klerk, *Green Chem.*, 2008, **10**, 1249.
4 S. K. Beaumont, *Phys. Chem. Chem. Phys.*, 2014, **16**, 5034.
5 Q. Zhang, J. Kang and Y. Wang, *ChemCatChem*, 2010, **2**, 1030.
6 Q. Zhang, K. Cheng, J. Kang, W. Deng and Y. Wang, *ChemSusChem*, 2014, **7**, 1251.
7 X. Li, J. He, M. Meng, Y. Yoneyama and N. Tsubaki, *J. Catal.*, 2009, **265**, 26–34.
8 J.-C. Kim, S. Lee, K. Cho, K. Na, C. Lee and R. Ryoo, *ACS Catal.*, 2014, **4**, 3919.
9 A. Y. Khodakov, W. Chu and P. Fongarland, *Chem. Rev.*, 2007, **107**, 1692.
10 K. Shimura, T. Miyazawa, T. Hanaoka and S. Hirata, *Appl. Catal., A*, 2014, **475**, 1.
11 G. Jacobs, T. K. Das, Y. Zhang, J. Li, G. Racoillet and B. H. Davis, *Appl. Catal., A*, 2002, **233**, 263.
12 Y. Ohtsuka, T. Arai, S. Takasaki and N. Tsubouchi, *Energy Fuels*, 2003, **17**, 804.
13 G.-Z. Bian, N. Fujishita, T. Mochizuki, W.-S. Ning and M. Yamada, *Appl. Catal., A*, 2003, **252**, 251.
14 A. Y. Khodakov, *Catal. Today*, 2009, **144**, 251.
15 R. Schlögl and S. B. A. Hamid, *Angew. Chem., Int. Ed.*, 2004, **43**, 1628.
16 C. Descorme, P. Gallezot, C. Geantet and C. George, *ChemCatChem*, 2012, **4**, 1897.
17 V. Polshettiwar and R. S. Varma, *Green Chem.*, 2010, **12**, 743.
18 Y. Li, Q. Liu and W. Shen, *Dalton Trans.*, 2011, **40**, 5811.
19 J. Sun and X. Bao, *Chem.–Eur. J.*, 2008, **14**, 7478.
20 J. K. Nørskov, T. Bligaard, J. Rossmeisl and C. H. Christensen, *Nat. Chem.*, 2009, **1**, 37.
21 S. Shylesh, V. Schiinemann and W. R. Thiel, *Angew. Chem., Int. Ed.*, 2010, **49**, 3428.
22 S. Chaturvedi, P. N. Dave and N. L. Shah, *J. Saudi Chem. Soc.*, 2012, **16**, 307.
23 G. A. Somorjai, H. Frei and J. Y. Park, *J. Am. Chem. Soc.*, 2009, **131**, 16589.
24 J. Schällibaum, F. H. D. Torre, W. R. Caseri and J. F. Löffler, *Nanoscale*, 2009, **1**, 374.
25 C. Yang, H. Zhao, Y. Hou and D. Ma, *J. Am. Chem. Soc.*, 2012, **134**, 15814.
26 H. R. Choi, H. Woo, S. Jang, J. Y. Cheon, C. Kim, J. Park, K. H. Park and S. H. Joo, *ChemCatChem*, 2012, **4**, 1587.
27 T. M. Eggenhuisen, J. P. den Breejen, D. Verdoes, P. E. de Jongh and K. P. de Jong, *J. Am. Chem. Soc.*, 2010, **132**, 18318.
28 M. Trueba and S. P. Trasatti, *Eur. J. Inorg. Chem.*, 2005, 3393.
29 I. Puskas and R. S. Hurlbut, *Catal. Today*, 2003, **84**, 99.
30 O. O. James, B. Chowdhury, M. A. Mesubi and S. Maity, *RSC Adv.*, 2012, **2**, 7347.